Journal of
Ceramic Science
and Technology

J. Ceram. Sci. Technol., **11** [2] 91-98 (2020)
DOI: 10.4416/JCST2020-00010
available online at: http://www.ceramic-science.com

Densification of Mn-Doped YSZ for the Solid Oxide Membrane Process and its Surface Corrosion under Fluoride Salt

J. Kanghee[1], K. Buyoung[2], R. Jiseung[3], K. Hyeong-Tae[4], L. Heesoo[*1]

[1]School of Materials Science and Engineering, Pusan National University, Busan, 46241, Republic of Korea
[2]Department of Research and Development, HyMAR Corporation, Busan, 46241, Republic of Korea
[3]Analysis Technology Center, Korea Institute of Ceramic Engineering and Technology, Jinju-si, Gyeongsangnam-do, 52851, Republic of Korea
[4]Engineering Ceramic Center, Korea Institute of Ceramic Engineering and Technology Icheon Branch Institute, Icheon-si, Gyeonggi-do, 17303, Republic of Korea
received January 30, 2020; received in revised form July 29, 2020; accepted August 9, 2020

Abstract

The densification-induced changes in the crystal structure and microstructure of *x* mol% Mn-doped 8YSZ (*x*Mn-YSZ, *x* = 0, 0.5, 1.0, or 2.0) were investigated, and the mechanical and electrical properties of the samples were determined to evaluate their chemical degradation resulting from chemical stress loading. The *x*Mn-YSZ samples synthesized with a solid-state reaction method possessed cubic crystal structures, similar to 8YSZ. The 0.5Mn-YSZ (111) peak shifted to a lower angle compared to that of YSZ. As the content of Mn increased, the *x*Mn-YSZ peak gradually shifted to higher angles. The peak shift was attributed to lattice shrinkage (after expansion) with increasing Mn content. The grain size and porosity of YSZ were 9.07 µm and 1.21 %, respectively, and those of 0.5Mn-YSZ were 21.90 µm and 0.63 % respectively, revealing that Mn doping led to densification. The hardness increased to 2065.92 Hv (2.0Mn-YSZ) with increasing Mn content, similar to density. Because of the complex effects of densification and lattice distortion, the polarization resistance decreased to 48 % of YSZ for 0.5Mn-YSZ; however, the resistance gradually increased with increasing Mn content. After NaF-CaF_2 was loaded as a chemical stress, the cubic and tetragonal phases destabilized and the porosity increased to 2.80 % and 5.44 % for 1.0Mn-YSZ and 2.0Mn-YSZ, respectively. On the other hand, 0.5Mn-YSZ without the tetragonal phase showed a porosity of 2.25 %, indicating that a Mn doping content of > 2.0 mol% worsened YSZ corrosion.

Keywords: Mn-doped YSZ, sinterability, polarization resistance, fluoride salt, surface corrosion, destabilization

I. Introduction

The solid oxide membrane (SOM) process is a technique utilized to separate oxygen from oxides such as MgO and InO with a salt bath containing Cl^- and F^- ions and convert the oxides to the corresponding metals. Yttrium-stabilized ZrO_2 (YSZ), an oxygen ion conductor, is considered an alternative to previously used graphite electrodes that are prone to oxygen ion corrosion in the salt bath [1,2]. YSZ exhibits high ionic conductivity and thermal and chemical stability at 800 – 1 000 °C, and is widely used in the SOM process, solid oxide fuel cell electrolytes, oxygen sensors, and thermal barrier coatings (TBCs) [3–6]. However, the harsh operating environment of SOMs or TBCs causes corrosion because of the persistent chemical and thermal stresses.

In the SOM electrolysis process, the Cl^- and F^- ions in the salt bath act as a strong source of stress. Various studies have been conducted to suppress the stress. For instance, Milshtein *et al.* inhibited corrosion by pre-injecting the corrosion product, YF_3 [7]. Zuo *et al.* added a less reactive element to the stress source [1]. In addition, some studies have been conducted to improve the corrosion resistance by controlling the reactivity based on grain size adjustment. Changing the heat treatment profile or inducing densification by liquid phase sintering by means of doping of transition metal oxides has been attempted to adjust the grain size [8–12]. Therefore, understanding the relation between the variation in the sintering characteristics of zirconia by means of grain size adjustment and the corrosion behavior is important in the SOM electrolysis process.

We investigated the grain size and density changes of 8YSZ after MnO_2 doping and examined the changes in the various characteristics resulting from the application of a chemical stress (fluoride salt). Doping of Mn into YSZ resulted in a change in the crystal structure. The densification behavior, and physical, mechanical and electrical characteristics, such as density, surface morphology, porosity, polarization resistance, and hardness, were observed. A chemical stress was applied to both YSZ and Mn-doped YSZ samples. Changes in various characteristics, including the sintering behavior, mechanical and electrical properties, and crystal structure, and degradation caused by the fluoride salt were investigated.

* Corresponding author: heesoo@pusan.ac.kr

II. Experimental

Commercial Tosoh YSZ powder (TZ-8Y, Tosoh Corporation) and MnO_2 powder (Junsei Chemical Co. Ltd.) were prepared according to the composition (0.5, 1.0, and 2.0 mol% Mn-YSZ). Then, the powders were ball-milled for 24 h and calcined at 950 °C for 2 h. Next, the disk specimens (Ø 25 mm × ~ 2.5 mm thick) and the bar-type specimens (3.5 mm × 4.5 mm × 36 mm) were uniaxially pressed at 3.2 ton/m^2 in a steel die. During sintering, the samples were heated up to 1 600 °C with a heating rate of 5 K/min and held at this temperature for 6 h. Then the samples were cooled to the ambient temperature in air. The flexural strength samples were pressed and fabricated according to the same sintering schedule.

The chemical stress loading test was conducted using the eutectic composition of calcium fluoride (98 %, Junsei Chemical Co. Ltd.) and sodium fluoride (98 %, Junsei Chemical Co. Ltd.) by ball milling at 200 rpm in Nalgene bottles for 12 h. Then, typically, 0.7 g of the mixed powder was pelletized (1 ton/m^2) in a cylindrical 10-mm die. The obtained fluoride composite green bodies were then attached to the surfaces of Mn-YSZ discs and heated at 900 °C for 100 h.

The X-ray diffraction (XRD) patterns of Mn-doped and degraded powders were collected at room temperature with a step scan procedure (2θ = 20 – 80°, step interval: 0.02°, CuKα radiation, Rigaku Ultima-IV, Rigaku). The sample surfaces were observed by means of field-emission scanning electron microscopy (FESEM, MIRA3, TESCAN). The grain size was determined from the SEM images based on ISO 13383 – 1 [13]. The grain size was defined as the diameter of the circumscribed circle from image analysis. The porosities and densities of Mn-doped and degraded samples were measured with the Archimedes' method (XS205, Mettler Toledo). AC impedance measurements were performed with IviumStat (Ivium, Netherlands) in the frequency range from 10^6 Hz to 10^{-2} Hz using an excitation voltage of 10 mV at an operating temperature of 1 000 °C in air. The polarization resistance values were determined from the differences between the high- and low-frequency intercepts of the impedance spectra for all specimens. A nanoindenter (FISCHERSCOPE, HM2000, Germany) was used to measure the Vickers hardness. The measurement was conducted under a maximum load of 120 mN, applied for 5 s. The hardness was measured three times before and after chemical stress loading, and the average value was used. Flexural strength was measured with the three-point bending method using test specimens measuring 3.5 mm × 4.5 mm × 36 mm according to ISO 14704 [14]. The tests were carried out at ambient temperature using a universal testing machine with a loading rate of 0.5 mm/min and a span of 30 mm. Reported strengths represented the average value and standard deviation of five specimens.

III. Results and Discussion

(1) Sintering behavior

We analyzed the XRD patterns of Mn-doped YSZ (*x*Mn-YSZ) samples, as shown in Fig. 1. All specimens exhibited cubic structures, similar to fully stabilized zirconia. However, slight peak shifts were observed (see Fig. 1(a)). Compared to those of YSZ, the main peaks of *x*Mn-YSZ samples (Fig. 1(b)) shifted to lower angles; the peak shift for 0.5Mn-YSZ was 0.15°, and with increasing Mn content, the peak gradually moved to higher angles. The main peaks of 1.0Mn-YSZ peak and YSZ coincided, and the 2.0Mn-YSZ peak shifted to a higher angle by 0.12°. Clavel *et al.* reported that in samples with < 1.4 % Mn content, Mn predominantly exists as Mn^{2+} (96 pm), which is larger than Zr^{4+} (84 pm). However, as the content of Mn increases, Mn predominantly exists as Mn^{3+} (64.5 pm), which is smaller than Mn^{2+}, resulting in lattice distortion, wherein the lattice shrinks after expanding [15]. The Mn^{2+} ion predominantly exists at low doping levels, which is larger than Zr^{4+}. On the other hand, as the doping amount gradually increases, the fraction of Mn^{3+} smaller than Zr^{4+} increases. The XRD peak gradually shifts to a higher angle after it shifts to a lower angle, accordingly.

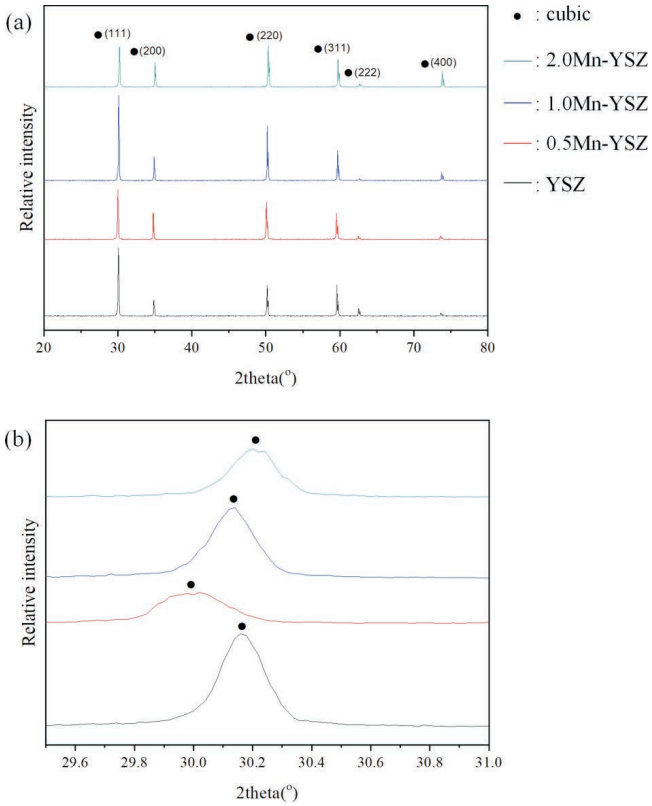

Fig. 1: (a) XRD patterns and (b) (111) peaks of YSZ and Mn-doped YSZ.

Fig. 2 shows the SEM images and average grain sizes of sintered *x*Mn-YSZ samples. The average grain sizes of YSZ, 0.5Mn-YSZ, 1.0Mn-YSZ, and 2.0Mn-YSZ were 9.07, 21.90, 23.19, and 26.46 μm, respectively. Thus, the grain size drastically increased at 0.5 mol% Mn doping and with further increase in the doping content, the grain size steadily increased. Fig. 3 shows the variation in the porosity and density with the Mn content. The porosity of YSZ was 1.21 %, and it significantly decreased to 0.63 % for 0.5Mn-YSZ. For 1.0Mn-YSZ and 2.0Mn-YSZ, the porosities were 0.52 % and 0.44 %, respectively, indicating the occurrence of densification. Zhang *et al.* reported that

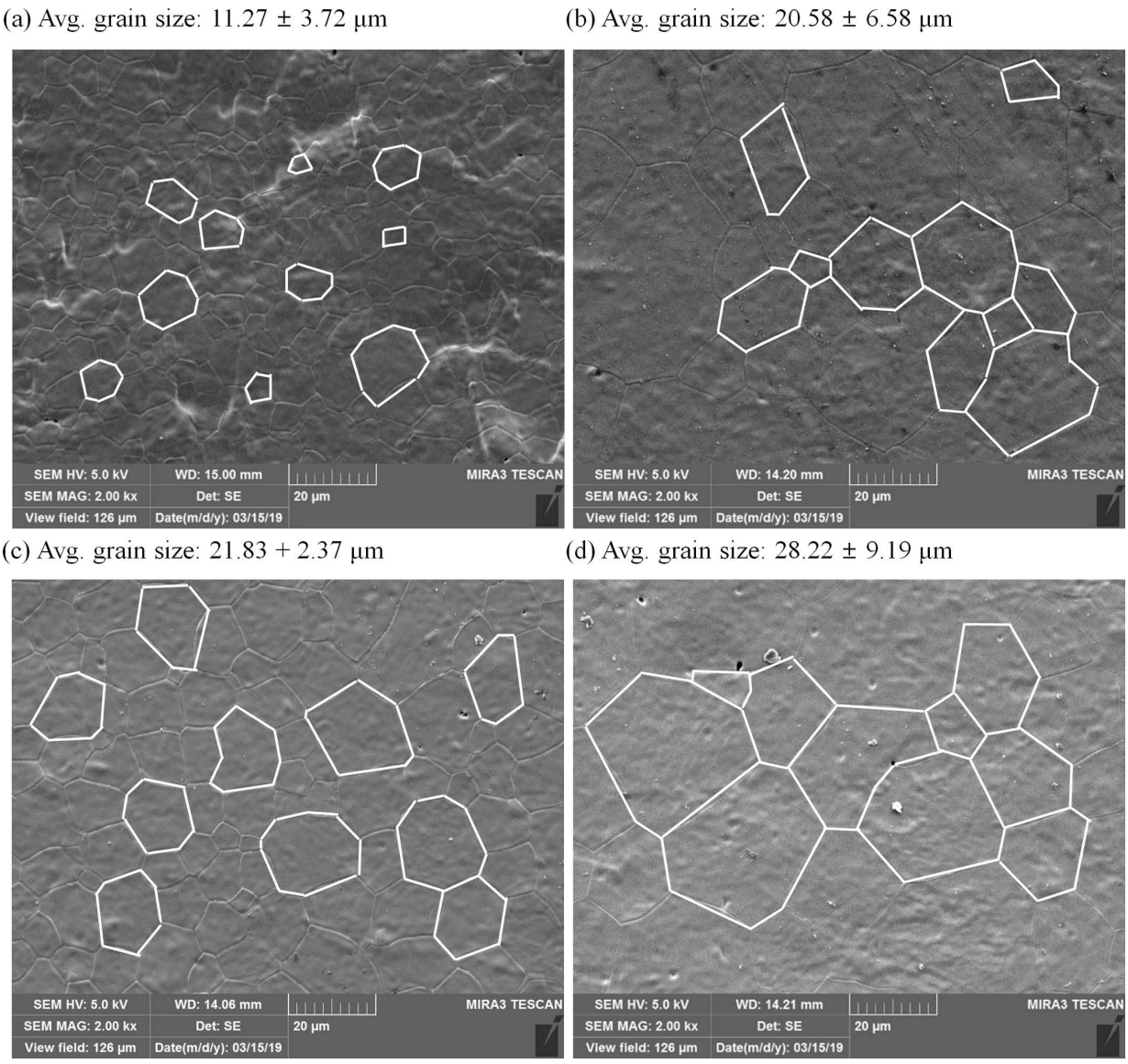

Fig. 2: SEM images of sintered specimens: (a) YSZ, (b) 0.5Mn-YSZ, (c) 1.0Mn-YSZ, and (d) 2.0Mn-YSZ. .

MnO_2 acted as a sintering additive similar to Fe_2O_3, inducing densification of YSZ. With densification of *x*Mn-YSZ, the density increased up to 6.27 g/cm^3 [9]. As the content of Mn increases, the amount of liquid while sintering is increased, resulting in densification to 6.27 g/cm^3.

The hardness and polarization resistance are shown in Fig. 4, confirming the effect of densification. As shown in Fig. 4(a), the mechanical properties of *x*Mn-YSZ samples steadily increased for the hardness from 1728.68 Hv to 2065.92 Hv and for the flexural strength from 57.52 MPa to 89.64 MPa owing to densification with the addition of Mn [8]. Fig. 4(b) shows the polarization resistance of *x*Mn-YSZ samples at 1 000 °C. The polarization resistance decreased from 64.55 Ω cm^2 for YSZ to 31.06 Ω cm^2 for 0.5Mn-YSZ; however, with further increase in the Mn content, the polarization resistance increased to 40.60 Ω cm^2 and 51.72 Ω cm^2 for 1.0Mn-YSZ and 2.0Mn-YSZ, respectively. The polarization resistance of zirconia is composed of intragranular resistance and grain boundary resistance, which depend on the microstructure and lattice distortion. The polarization resistance of 0.5Mn-YSZ was lower than that of YSZ because of the larger grain size of 0.5Mn-YSZ. With an increase in the Mn doping content, which caused lattice distortion, the polarization resistance increased [10].

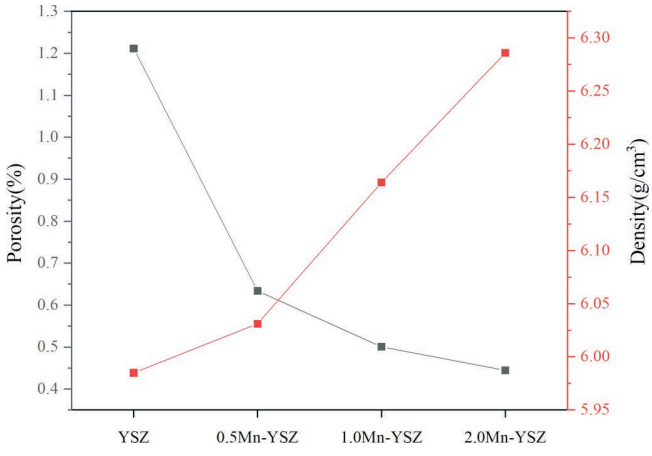

Fig. 3: Porosity and density of YSZ and Mn-doped YSZ.

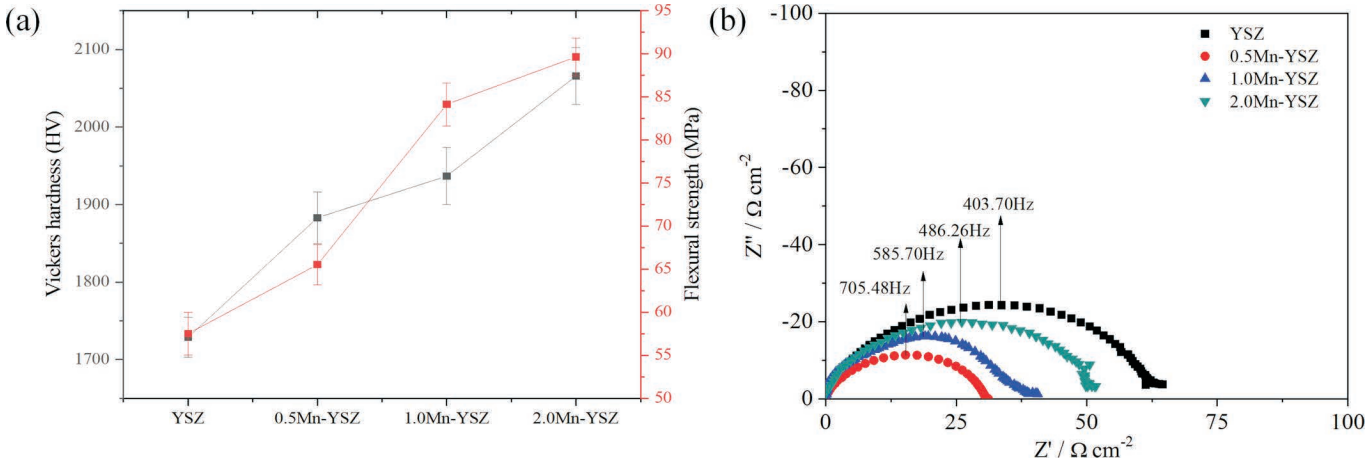

Fig. 4: (a) Hardness and flexural strength and (b) polarization resistance of YSZ and Mn-doped YSZ.

To summarize, compared to those of YSZ, the sintering properties of 0.5Mn-YSZ were drastically improved. However, with further increase in the Mn content, the sintering properties gradually improved, and the lattice gradually distorted because of the change in the valence state of Mn. Moreover, because of densification, the hardness of *x*Mn-YSZ samples was higher than that of YSZ. Furthermore, the polarization resistance decreased with 0.5 mol% Mn doping (0.5Mn-YSZ), but it gradually increased with further increase in the Mn content to 1.0 mol% and 2.0 mol% because of lattice distortion.

(2) Surface corrosion

The XRD patterns of *x*Mn-YSZ samples after fluoride salt loading (i.e. chemical stress) are presented in Fig. 5. At $x = 0$ and 0.5, the cubic phase was retained. However, phase separation into cubic and tetragonal phases was observed for 1.0Mn-YSZ and 2.0Mn-YSZ. This implies that the F^- ion in the molten salt reacted with the zirconia stabilizer, as shown in Eq. (1), resulting in destabilization. Notably, Mn ions were more easily depleted than yttrium ions because the bonding enthalpy of Mn-O (402.00 kJ/mol) was lower than that of Y-O (715.16 kJ/mol) [16]. This could be the effect of lattice distortion induced by Mn doping and the bonding enthalpy difference between Mn-O and Y-O [1].

$$Y_2O_{3,\ YSZ} + 6F^- \rightarrow 2YF_{3,\ flux} + 6O^{2-} \qquad (1)$$

As shown in Fig. 6, grain boundaries were hardly observed in the samples; however, all specimens exhibited microcracks. As reported by Guo *et al.* and Eklund *et al.* [17, 18], the stabilizer ions in the specimens were eluted by fluoride ions, resulting in the formation of an yttrium depletion layer. The yttrium depletion layer contained small amounts of the monoclinic phase, which had a density of 5.68 g/cm^3. Microcracks were formed at the interface between the flux and the specimen because of the density difference between the monoclinic and cubic phases. Subsequently, the region containing microcracks widened, and gradually, cracks were formed in the inner regions of the specimens. The porosity and density changes caused by chemical stress loading are shown in Fig. 7. As the content of Mn increased, the porosity increased; the porosities of YSZ, 0.5Mn-YSZ, 1.0Mn-YSZ, and 2.0Mn-YSZ were 2.50, 2.25, 2.80, and 5.44 %, respectively, and these values were higher than those before the application of chemical stress. Thus, the porosity increased with increasing Mn content, opposite to that observed before the chemical stress loading. As mentioned above, Mn ions were easily depleted because of the weak Mn-O bond.

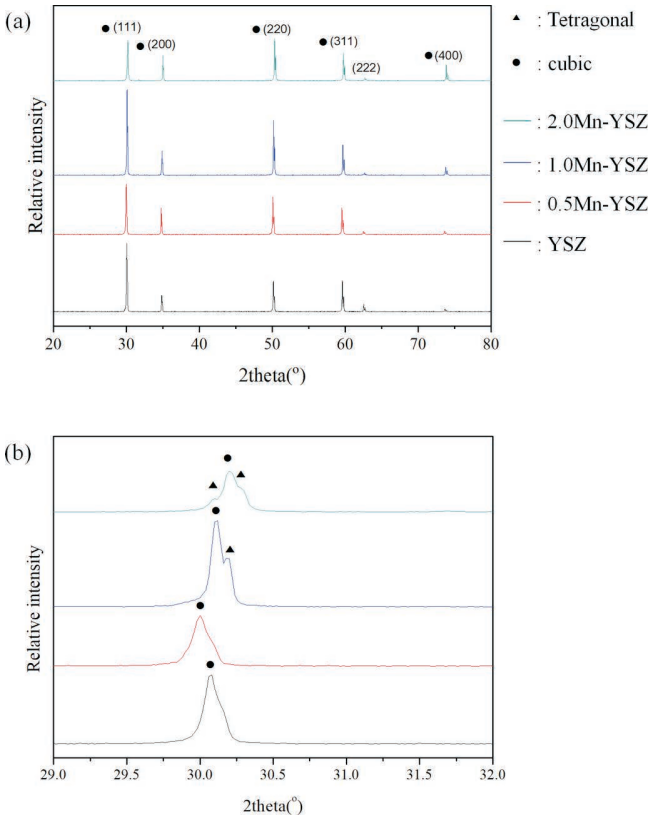

Fig. 5: (a) XRD patterns and (b) (111) peaks of YSZ and Mn-doped YSZ after chemical stress loading.

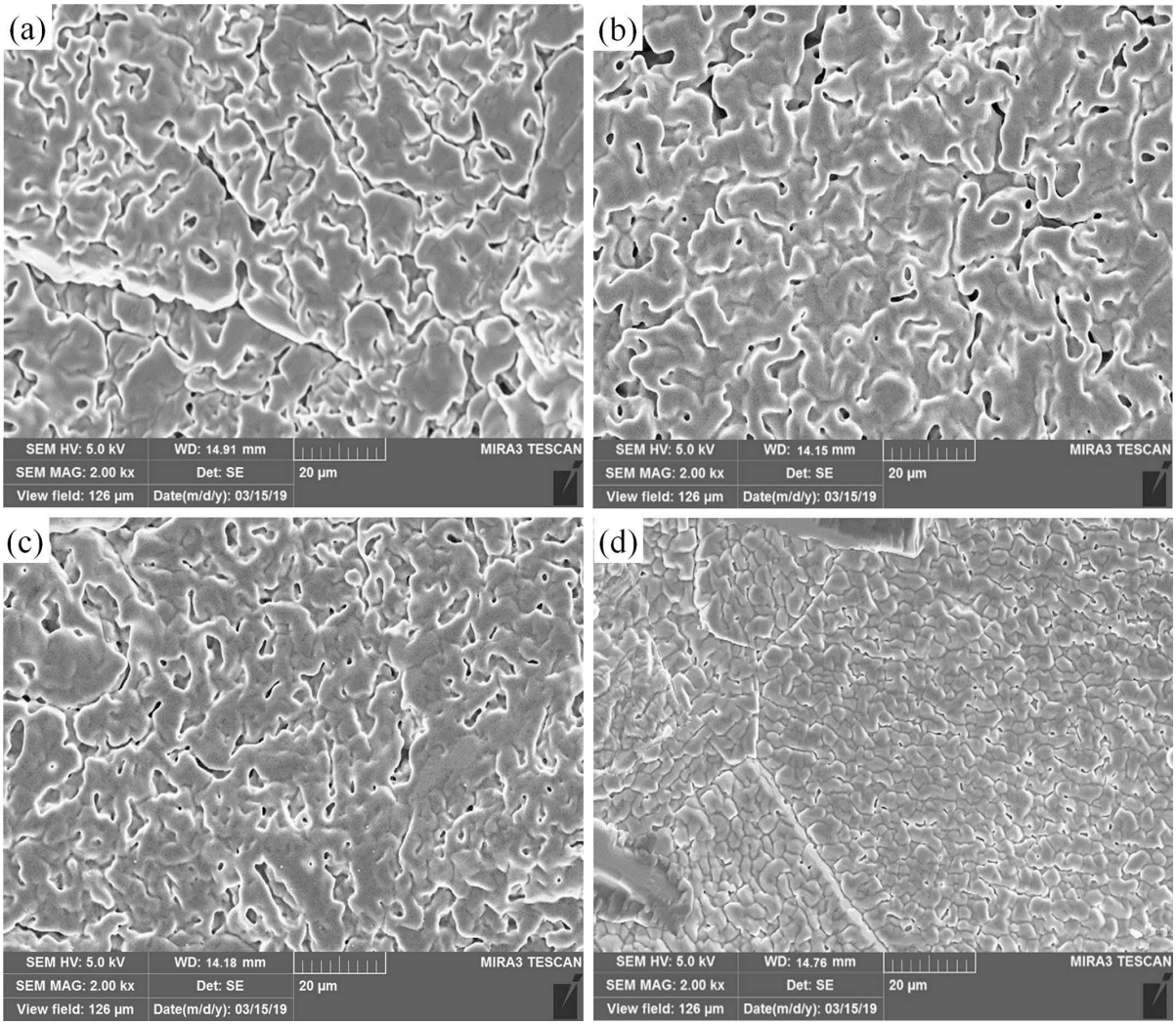

Fig. 6: SEM images of specimens after chemical stress loading: (a) YSZ, (b) 0.5Mn-YSZ, (c) 1.0Mn-YSZ, and (d) 2.0Mn-YSZ.

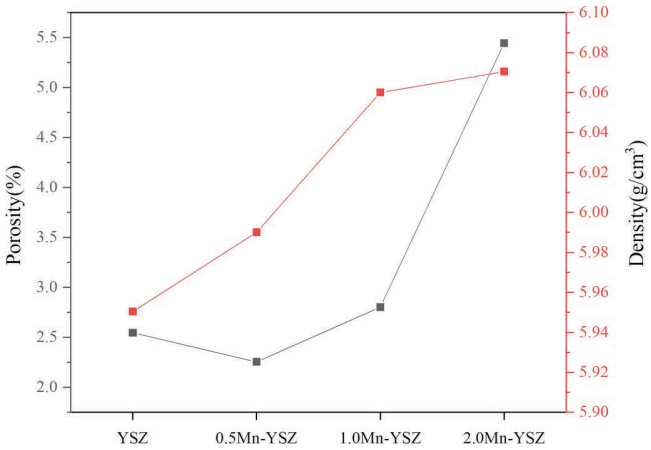

Fig. 7: Porosity and density of YSZ and Mn-doped YSZ after chemical stress loading.

Fig. 8(a) shows the hardness of *x*Mn-YSZ samples after chemical stress loading. The hardness decreased from 1903.57 Hv to 1202.82 Hv on average, opposite to that before the chemical stress loading. And the flexural strength of Mn-YSZ showed similar values, 55.41, 55.89, 62.75 MPa for 0.5, 1.0 and 2.0Mn-YSZ, with YSZ before chemical stress loading. However, the hardness increased with increasing Mn content after the chemical stress loading. Fig. 8(b) shows the polarization resistance values of *x*Mn-YSZ samples after chemical stress loading. The polarization resistance gradually increased with increasing Mn content: 89.43, 133.90, 320.04, and 629.48 Ω cm^2 for YSZ, 0.5Mn-YSZ, 1.0Mn-YSZ, and 2.0Mn-YSZ, respectively. The increase in the polarization resistance was mainly attributed to the increase in the porosity. The tetragonal phase, which underwent destabilization, contributed to a marked increase in the polarization resistance of 1.0Mn-YSZ and 2.0Mn-YSZ by 7.88 and 12.17 times, respectively.

The *x*Mn-YSZ started to crack on the surface of the specimen owing to chemical corrosion caused by the fluoride salt, resulting in degradation of the mechanical and electrical properties. When the material is applied to a SOM tube, fracture is more easily caused by cracks on the surface of the specimen. Densification caused by the addition of Mn can reduce or suppress fracture by improving the mechanical properties. However, if more than 1.0 mol% of Mn is added, the electrical property of the material is decreased before chemical degradation, and the efficiency may decrease when applied to the SOM process. 1.0 and 2.0Mn-YSZ after chemical degradation showed flexural strength of 58.89 and 62.75 MPa, respectively, and higher than the as-prepared YSZ (57.52 MPa).

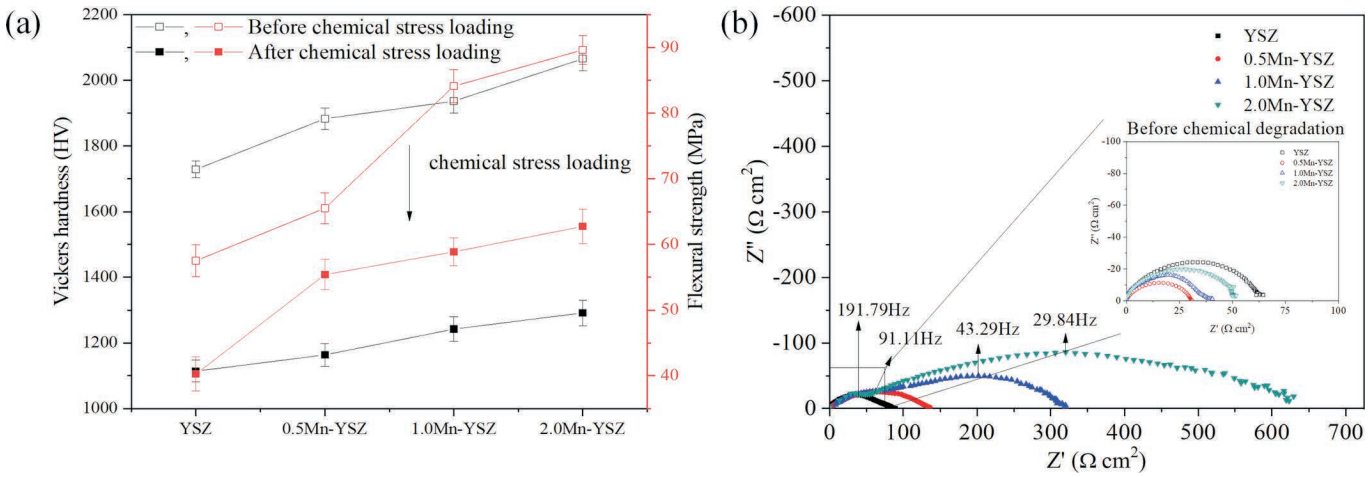

Fig. 8: (a) Hardness and flexural strength and (b) polarization resistance of YSZ and Mn-doped YSZ before and after chemical stress loading.

IV. Conclusions

8YSZ was doped with MnO_2 to induce densification. In addition, a fluoride salt was added to the samples, and to investigate the chemical corrosion caused by a fluoride salt, the electrical and mechanical properties of the samples were investigated. The crystal structure of Mn-YSZ gradually distorted because of the ionic radius change caused by Mn doping. The porosity of 8YSZ drastically decreased by 48 % after doping with 0.5% Mn (0.5Mn-YSZ), and it gradually decreased with increasing Mn content. Because of densification of *x*Mn-YSZ samples, the average grain size increased to 21.90 μm (0.5Mn-YSZ), 23.19 μm (1.0Mn-YSZ), and 26.46 μm (2.0Mn-YSZ). In addition, the hardness increased to 2065.92 Hv for 2.0Mn-YSZ. Moreover, the polarization resistance decreased to 31.06 Ω cm^2 for 0.5Mn-YSZ because of the reduced grain boundary fraction. However, with increasing Mn content, the polarization resistance increased (51.72 Ω cm^2 for 2.0Mn-YSZ) because of the resulting lattice distortion. Owing to corrosion, Mn was more easily depleted than Y. Notably, phase separation into cubic and tetragonal phases occurred at 1.0 mol% Mn doping. The porosity gradually increased from 2.25 % for 0.5Mn-YSZ to 5.44 % for 2.0Mn-YSZ after chemical stress loading. In addition, for 1.0Mn-YSZ and 2.0Mn-YSZ, the polarization resistance increased by 7.88 and 12.17 times, respectively. The hardness decreased from 1903.57 Hv to 1202.82 Hv on average compared to that before corrosion and the flexural strength of Mn-doped YSZ after chemical degradation showed values similar to or higher than those of the as-prepared YSZ. In the future, we plan to study the lattice distortion caused by Mn doping into stabilized zirconia in terms of the local atomic structure.

Acknowledgements

This work was supported by the Technology Innovation Program (10063427, Development of eco-friendly smelting technology for the production of rare metal production for lowering manufacturing costs using solid oxide membrane) funded by the Ministry of Trade, Industry & Energy (MOTIE, Korea).

References

1 Zou, X., Li, X., Shen, B., Lu, X., Xu, Q., Zhou, Z., Ding, W.: CeO 2-Y 2 O 3-ZrO 2 membrane with enhanced molten salt corrosion resistance for solid oxide membrane (SOM) electrolysis process, *Metall. Mater. Trans. B*, **48**, [1], 678–691, (2017).

2 Fray, D., Schwandt, C.: Aspects of the application of electrochemistry to the extraction of titanium and its applications, *Mater Trans*, **58**, [3], 306–312, (2017).

3 Chen, L.B.: Yttria-stabilized zirconia thermal barrier coatings—a review, *Surf. Rev. Lett.*, **13**, [5], 535–544, (2006).

4 Lee, D.H., Kim, T.W., Lee, K.S., Kim, C.: Thermal shock resistance of bilayered YSZ thermal barrier coating, *J. Kor. Ceram. Soc.*, **55**, [5], 452–460, (2018).

5 Han, M., Tang, X., Yin, H., Peng, S.: Fabrication, microstructure and properties of a YSZ electrolyte for SOFCs, *J. Power Sources*, **165**, [2], 757–763, (2007).

6 Park, H.W., Lee, Y.J., Kim, J.H., Jeon, D.W., Hwang, H.J., Lee, M.J.: Effect of reaction conditions on the particle properties for synthesis of stabilized zirconia by modified oxalate method, *J. Kor. Ceram. Soc.*, **53**, [5], 529–534, (2016).

7 Milshtein, J., Gratz, E., Pati, S., Powell, A.C., Pal, U.: Yttria stabilized zirconia membrane stability in molten fluoride fluxes for low-carbon magnesium production by the SOM process, *J. Min. Metall. B*, **49**, [2], 183–190, (2013).

8 Chong, F.D., Tan, C.Y., Singh, R., Muchtar, A., Somalu, M.R., Ng, C.K., Tan, Y.M.: Effect of manganese oxide on the sinterability of 8 mol% yttria-stabilized zirconia, *Mater. Charact.*, **120**, 331–336, (2016).

9 Zhang, T.S., Du, Z.H., Li, S., Kong, L.B., Song, X.C., Lu, J., Ma, J.: Transitional metal-doped 8 mol% yttria-stabilized zirconia electrolytes, *Solid State Ionics*, **180**, [23–25], 1311–1317, (2009).

10 Flegler, A.J., Burye, T.E., Yang, Q., Nicholas, J.D.: Cubic yttria stabilized zirconia sintering additive impacts: a comparative study, *Ceram. Int.*, **40**, [10], 16323–16335, (2014).

11 Nandy, A., Tiwary, C.S., Dutta, A., Chattopadhyay, K., Pradhan, S.K.: Effect of manganese (II) oxide on microstructure and ionic transport properties of nanostructured cubic zirconia, *Electrochim. Acta*, **170**, 360–368, (2015).

12 Zhang, T., Hing, P., Huang, H., Kilner, J.: Sintering study on commercial CeO_2 powder with small amount of MnO_2 doping, *Mater. Lett.*, **57**, [2], 507–512, (2002).

13 International standards organization. Fine ceramics (advanced ceramics, advanced technical ceramics) – microstructural characterization -- Part 1: determination of grain size and size dis-

tribution. ISO 13383 – 1. Geneva: International Standards Organization (ISO); 2012.

[14] International standards organization. Fine ceramics (advanced ceramics, advanced technical ceramics) – test method for flexural strength of monolithic ceramics at room temperature. ISO 14704. Geneva: International Standards Organization (ISO); 2016.

[15] Clavel, G., Willinger, M.G., Zitoun, D., Pinna, N.: Manganese-doped zirconia nanocrystals, *Eur. J. Inorg. Chem.*, **2008**, [6], 863 – 868, (2008).

[16] Chase, M.W., NIST-JANAF Thermochemical Tables, 4th Ed.; *J. Phys. Chem. Ref. Data Monogr*. 9, 1999.

[17] Guo, J., Villalon, T., Pal, U., Basu, S.: Effect of optical basicity on the stability of yttria-stabilized zirconia in contact with molten oxy-fluoride flux, *J. Am. Ceram. Soc.*, **101**, [8], 3605 – 3616, (2018).

[18] Eklund, S.E., Toth, L.M., Chambers, J.Q., Mamantov, G.: Determination of oxide in fluoride salts using an yttria-stabilized-zirconia oxygen pump, *Anal. Chem.*, **71**, [3] (1999).